Predicting the Wake Structure of the HART II rotor using the Vorticity Transport Model

Mary E. Kelly* and Richard E. Brown†
Department of Aerospace Engineering
University of Glasgow, Glasgow, G12 8QQ
mkelly@aero.gla.ac.uk, rbrown@aero.gla.ac.uk

ABSTRACT

Brown's Vorticity Transport Model has been used to predict the wake structure and resultant blade loading of the rotor that was studied during the HART II experimental programme. The descending flight condition of the experiment yields significant high-frequency content to the blade loading due to the presence of blade-vortex interactions. PIV images of the wake structure were compared against numerical predictions of the detailed geometry of the rotor wake using three different computational resolutions of the flow. This was done to investigate the origin of inaccuracies exposed in an earlier study of the system in capturing the effects of blade vortex interactions on the loading on the rotor. The predicted positions of the vortex cores agree with measured data to within a fraction of the blade chord, and the strength of the vortices is preserved to well downstream of the rotor, essentially independently of the resolution of the calculation. Nevertheless the amplitude of the loading impulses induced on the blade by vortex interaction are strongly influenced by the resolution of the calculation through the effect of cell density on the minimum vortex core size that can be supported. It would appear thus that the inaccuracies in predicting the high-frequency loading on the rotor are not due to any inherent deficiency in the representation of the wake, although viscous effects may need to be considered in future in order to decouple the vortex core size from the cell size, but rather due to the inherent deficiencies of the lifting line approach used to model the blade aerodynamics.

Nomenclature

a	Speed of sound
a_{ij}	Interpolation coefficients
c	Chord
C_N	Section normal force coefficient
C_T	Thrust coefficient, $T/\rho A(\Omega R)^2$
M	Mach number
N_a	Number of azimuthal interpolation functions
N_r	Number of radial interpolation functions
r	Non-dimensional radial coordinate
r_c	Vortex core radius
R	Rotor radius
S	Local vorticity source
t	Time
u	Flow velocity
u_b	Flow velocity relative to the blade
X	Wake streamwise coordinate
Y	Wake lateral coordinate
Z	Wake vertical coordinate
y_{el}	Elastic lag motion
z_{el}	Elastic flap motion
μ	Advance ratio
θ_{el}	Elastic blade torsion
ρ	Density
ω	Vorticity
ω_b	Bound vorticity
Ω	Rotor rotational velocity
ψ	Azimuth angle
Γ	Circulation

*Postgraduate Research Student
†Mechan Chair of Engineering

Presented at the 34th European Rotorcraft Forum, Liverpool, UK, 16–19 Sept. 2008.

Introduction

A particular source of helicopter vibration and noise, especially in descending flight or during manoeuvres, are the localised aerodynamic interactions between the rotor blades and the vortices that they

produce in their wake. Accurate prediction of the amplitude and position of the loading perturbations on the rotor that are induced by these blade-vortex interactions (BVI) relies critically upon the correct simulation of both the blade deformation and the position and strength of the vortical structures within the rotor wake. Modelling the evolution of the vortices within the wake, and capturing correctly their position and strength over time, is a particularly challenging task given the complex aerodynamic environment in which the helicopter rotor operates. The availability of a reliable tool that can predict accurately the high frequency components of the blade loading, particularly those that are responsible for the rather objectionable characteristics of the helicopter under certain flight conditions, would be of significant benefit to the designers of modern rotorcraft given the current industrial focus on reduction of both maintenance costs and noise. Accurate modelling of the structure of the wake generated by the helicopter rotor has thus become one of the primary challenges for the developers of Computational Fluid Dynamics (CFD) methods designed for rotorcraft applications.

CFD calculations of the flow around the entire rotorcraft, or even just the rotor, are extremely challenging however. This is because simultaneous accurate representation of flow features on the scale of the rotor (for instance the overall geometry of the wake) and of the vortex cores (for instance the details of the rollup process behind the blades that leads to the formation of the tip vortices) requires a method that can resolve the relevant physics over at least two spatial orders of magnitude. For most CFD methods, the accuracy of the solution is inevitably thus a trade-off between the need for high fidelity resolution of the wake and the computational cost that is incurred in achieving this fidelity. At present this compromise invariably results in solutions that are grid dependent since rotor calculations on grids that are sufficiently fine to resolve the detailed structure of the wake are usually prohibitive in terms of computational cost.

The Higher Harmonic Control Aeroacoustics Rotor Test (HART) programme (Refs. 1–4) was initiated to provide experimental insight into the structure of the rotor wake and its effect on the aerodynamic loading of the rotor blades and thus on the acoustic signature of the rotor. Three different flight cases were studied – a baseline case with conventional control inputs, and two cases with higher harmonic control inputs applied to the rotor, the so-called minimum vibration and minimum noise cases. The second HART test, in particular, concentrated on gathering detailed measurements of the rotor wake in order to catalogue the development of the blade-tip vortex as it ages and convects away from its point of origin. The three-component Particle Image Velocimetry (3C-PIV) technique that was used in the HART II tests allowed instantaneous measurement of the velocity field contained within a series of highly-resolved observation areas located at various positions near the rotor disc as illustrated in Fig. 1.

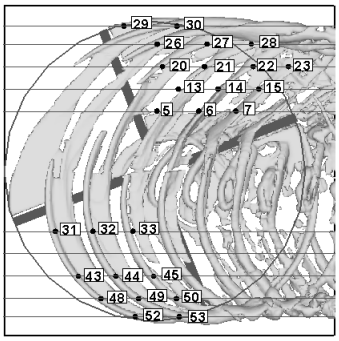

(a) *At 20 degrees azimuth*

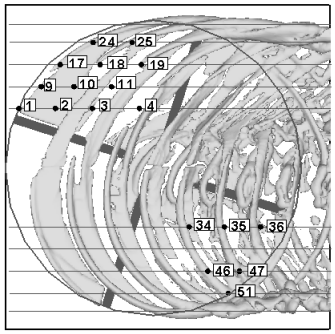

(b) *At 70 degrees azimuth*

Figure 1: *Locations of PIV measurement planes superimposed on the wake structure predicted by the VTM for the baseline HART II case,* $\mu = 0.15, C_T = 0.00457$.

In this paper, predictions of the wake structure of the HART II rotor, obtained using Brown's Vorticity Transport Model (VTM) are compared to the HART II experimental data set. The particular version of the VTM used in this study allowed the blade dynamics to be prescribed in order to isolate those modelling issues which relate to the aerodynamics of the system from those relating to the structural dynamics. The VTM is based on a time-dependent vorticity-velocity formulation of the Navier-Stokes equations, solved computationally on a structured grid system surrounding the rotor. The method has been designed specifically to reduce numerical dissipation of the vorticity in the flow and thus to maintain the compactness, over many rotor revolutions, of the vortical structures that are present in the rotor wake. This property of the model should, in principle, make the VTM particularly well suited to predicting loading

perturbations on the scale of blade-vortex interactions if care is taken to resolve the wake to a suitable level of precision and detail.

The VTM has been used previously to predict the geometry of the wake system, the resultant rotor blade loading and the radiation of acoustic noise for the HART II rotor (Ref. 5). This earlier investigation suggested that accurate prediction of the high-harmonic, BVI-induced component of the airloads on the rotor is greatly influenced by the accuracy to which the wake geometry can be resolved. Where the prediction of the strength and geometry of the wake was the most accurate, generally on the retreating side of the rotor, all BVI events discernible in the experimental data were reproduced in the numerical prediction of the blade loading, usually with the correct phase and often with the correct amplitude. Where the prediction of the strength and geometry of the wake was poorer, generally on the advancing side of the rotor, the numerical resolution of the BVI-induced loads was less accurate both in amplitude and phase. The principal discrepancies in airload, vortex position and acoustic prediction were confined almost exclusively to the rear of the advancing side of the rotor and, if errors in reproducing the deflections of the blades could be discounted, were thought to be due to minor inaccuracies in modelling the development of the rotor wake, particularly the rollup of the vortex sheet immediately behind the blades to form the tip vortices on the advancing side of the rotor disc. The present paper will examine the possible origins of these deficiencies by comparing the vortex geometry and vortex core characteristics predicted by the VTM to those recorded during the HART II rotor test.

Model parameters

The instrumented model rotor tested during the HART II programme was based on the characteristics of the Bö 105 main rotor. The four-bladed rotor was scaled both geometrically and aeroelastically to 40% of the full rotor size, giving a radius of 2m and a chord of 0.121m. The rotor blades had a NACA23012 aerofoil with the trailing edge modified to form a 5.4mm (4.46% chord) tab. They were rectangular in planform with square tip and had -8° of linear twist. The rotor was flown with a shaft tilt of 5.3° aft of the vertical and at an advance ratio of 0.15. This test condition corresponds to a typical noise certification condition for maximum BVI noise radiation. The operational parameters of the test are summarised in Table 1. A detailed description of the rotor model and the measurement procedures that were used in the HART II experiments are given in Refs. 1–4.

Table 1: Rotor operational parameters

Forward velocity	33 m/s
Rotational speed	1041 rpm
Blade passage Frequency	70 Hz
Shaft tilt	5.3° aft
Thrust coefficient	0.00457
Advance Ratio	0.15

Computational model

The present formulation of the Vorticity Transport Model (VTM), developed by Brown and Line (Refs. 6 and 7) couples a lifting-line model for the aerodynamics of the blade to an Eulerian representation of the vorticity in the flow field.

The flow field is evolved by solution of the Navier-Stokes equations in vorticity-velocity form on a structured Cartesian grid. Assuming incompressible flow with velocity u, the associated vorticity distribution $\omega = \nabla \times u$ evolves according to the unsteady vorticity transport equation

$$\frac{\partial}{\partial t}\omega + u \cdot \nabla\omega - \omega \cdot \nabla u = S + \nu\nabla^2\omega \qquad (1)$$

where ν is the viscosity of the fluid. The local rate of numerical diffusion is controlled very effectively by using a set of highly compressive flux limiters within the particular implementation of Toro's Weighted Average Flux method (Ref. 8) that is used within the code to convect the solution through time. At each time step, the velocity at the cell faces is obtained from the vorticity distribution using a fast multipole technique to invert the differential form of the Biot-Savart equation

$$\nabla^2 u = -\nabla \times \omega. \qquad (2)$$

A semi-Lagrangian adaptive grid is used to track the evolving vorticity in such a way that cells only exist in regions of the computational domain where the vorticity is non-zero. As the vorticity moves to a new location, new cells are created and any cells that no longer contain vorticity are destroyed. Thus, the grid structure is free to follow the evolution of the wake, eliminating the requirement for explicit numerical boundary conditions at the edge of the computational domain and increasing the computational efficiency of the method. Moreover, a nested grid system allows for fine resolution close to the rotor and then a systematic decrease in resolution with distance from the rotor hub.

An extension of the Weissinger-L formulation of lifting-line theory is implemented on a series of discrete panels along the length of each rotor blade to

yield the aerodynamic loading. A bound vortex is attached to the quarter-chord of each panel. The strength of the bound vorticity along the length of the blade is determined by enforcing, simultaneously, a condition of zero through-flow on a set of aerodynamic stations located at the 3/4 chord of each panel. As the computation is progressed through each time step, trailed and shed vorticity from each vortex panel is added to the near wake downstream of the blade as the local vorticity source,

$$S = -\frac{d}{dt}\omega_b + u_b \nabla \cdot \omega_b, \tag{3}$$

where ω_b is the bound vorticity. The two-dimensional aerodynamic characteristics of the rotor blade sections are specified in a look-up table as a function of angle of attack and Mach number for a given Reynolds number. These characteristics can be used to precondition the boundary condition that is applied at the control points to allow the lifting line calculation to match closely the sectional aerodynamic characteristics, including stall, of the actual blade. As this approach is still essentially inviscid, the profile drag of the blade is calculated as a separate function of local angle of attack and is then added to the local aerodynamic force that is calculated from the lifting line model.

Fuselages or other solid bodies are represented using an unsteady vortex panel method, as described in Ref. 9. The surface of any body immersed in the flow-field is discretised into a system of panels, such that each panel edge is represented as a vortex filament with constant strength, forming a closed loop of vorticity. The velocity at the centroid of any panel is calculated as the sum of the influences from all vortex filaments on the body together with the velocity induced by all the other vorticity within the flow. To determine the strengths of the vortex loops, a boundary condition of zero through-flow is enforced simultaneously at the centroids of all panels. In the simulations described in this paper, the drive housing for the HART II rotor was modelled using 1908 panels. This yields a level of resolution that is comparable to previous simulations using this approach, for example as described in Ref. 9.

In the particular version of the model used in this investigation, the motion of the blades is prescribed, based on a variable-separable interpolation of the blade deformations that were measured at discrete azimuthal and radial locations on each blade during the HART II experiment. Each component D of the deformation is reconstructed using the interpolating function

$$D(r,\psi) = \sum_{i=1}^{N_r}\sum_{j=1}^{N_a} a_{ij} R_i(r) P_j(\psi), \tag{4}$$

where N_r and N_a are respectively the number of radial and azimuthal interpolation functions $R_i(r)$ and $P_j(\psi)$ used to describe the particular component of the blade deflection. The radial interpolation functions were taken to be polynomials and the azimuthal interpolation functions were taken to be the components of a Fourier series so that

$$R_i(r) = r^{(i-1)} \tag{5}$$

and

$$P_j(\psi) = \begin{array}{cc} \cos\frac{j-1}{2}\psi & \text{if} \quad j \in \{1,3,5,\ldots\} \\ \sin\frac{j}{2}\psi & \text{if} \quad j \in \{2,4,6,\ldots\}. \end{array} \tag{6}$$

The coefficients a_{ij} of the interpolation function were calculated by enforcing a simple least squares fit to the measured data for the blade deformations. The sets of coefficients that give the best approximation to the elastic flap, lag and torsional deformations z_{el}, y_{el} and θ_{el} of the blades using six radial and nine azimuthal interpolation functions are given in Ref. 5 for the baseline, minimum vibration and minimum noise cases test cases.

In the HART II tests, the blade deformation was measured using a non-intrusive optical method, called Stereo Pattern Recognition, as described in Refs. 10–12. Reflective markers were attached to both the leading and trailing edges of all four blades at eighteen regular radial stations from 23% span to the blade tip. The positions of the markers were then recorded at 15° intervals of the blade azimuth. No data were taken at the zero azimuth position and there are missing data where the markers could not be viewed because they lay within the shadow of the drive enclosure and the mounting support, or because the markers had peeled off the blades. The measurements of blade deflection are thus relatively sparse and there are significant gaps in the data, which may reduce the reliability of the interpolation particularly in areas where large amounts of data are missing.

The difference between the interpolation and the experimental data set for each of the measured components of the elastic deformation of the blades was nevertheless within the stated error bounds on the measurements of ±0.5° for the elastic torsion and ±0.5mm for the flap and lag deflections. The sensitivity of the calculations to the number of interpolation functions used in the azimuthal direction to capture the structural deflection of the blades was investigated and very little change was observed in the predicted airloads when the number of azimuthal interpolating functions was increased from 9 to 13. The largest effects of changing the number of azimuthal interpolation functions were confined to the higher harmonic component of the loading at the rear of the rotor disc where, in any case, a number of missing markers rendered the accuracy of the interpolation most in doubt.

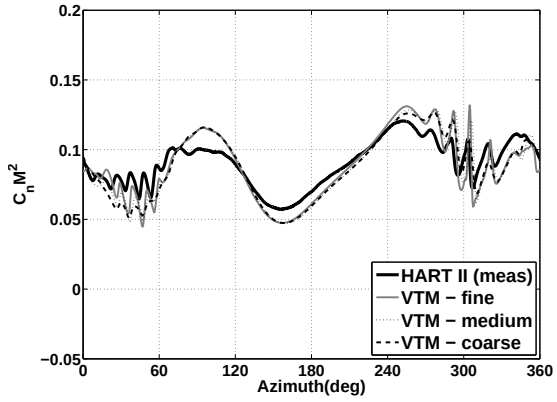

(a) *Full signal*

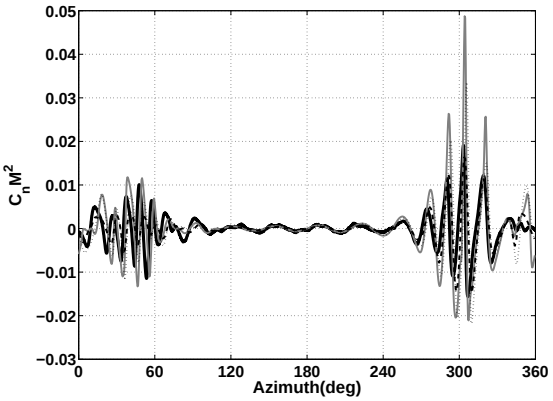

(b) *Signal filtered to include only the higher harmonic components (greater than 10 per rotor revolution)*

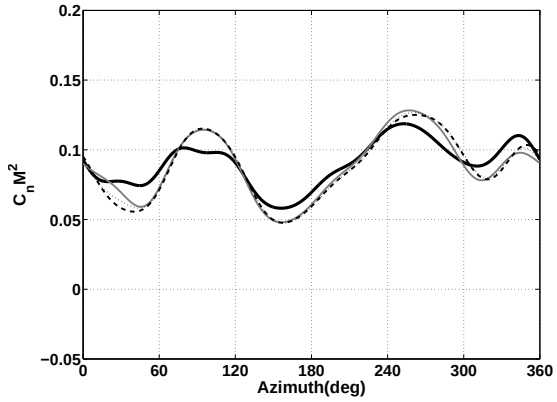

(c) *Signal filtered to include only the lower harmonic components (0-10 per rotor revolution)*

Figure 2: *Predicted Blade loading (C_NM^2) at 87% span, using various computational resolutions, compared to experimental data. Baseline HART II case.*

A prescription of the blade dynamics was also generated using the data synthesis method described by van der Wall in Ref. 13, where reconstruction of the blade dynamics was based on a best fit to the lowest pre-computed mode shapes for the structural deformation of the blades. The largest differences between the aerodynamic loads that result from using the two different methods of interpolation were found at the rear of the rotor disc (ψ =350° to 10°) in the higher harmonic signal where a slight change in the phase of the BVI impulses on the advancing side of the rotor disc was the most noticeable difference between the two sets of results. The similarity between the predictions that were obtained using the two different interpolations lends support to the validity of both approaches, however. In this paper, the results of VTM calculations at three different spatial and temporal resolutions (as summarised in Table 2) are compared to expose the effect of grid resolution on the ability of the method to predict the detailed structure of the wake of the HART II baseline case. Throughout, the structural dynamics of the blades were prescribed using six interpolation functions in the radial direction and nine in the azimuthal direction. The rotor was trimmed to the experimental thrust coefficient and to zero aerodynamic pitch and roll moments about the rotor hub.

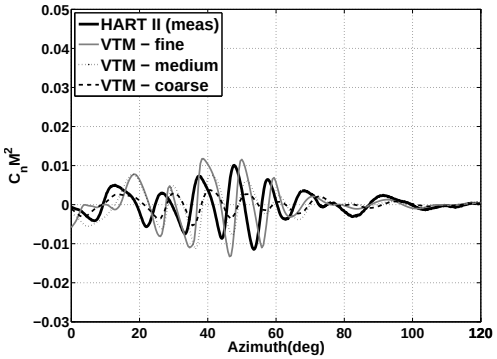

(a) *Advancing side of rotor disc*

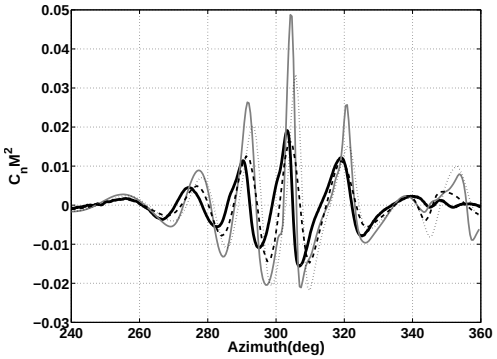

(b) *Retreating side of rotor disc*

Figure 3: *Predicted Blade loading (C_NM^2) at 87% span, using various computational resolutions, compared to experimental data. Signal filtered to include only higher harmonic components (greater than 10 per rotor revolution). Baseline HART II case.*

Table 2: Computational Resolution

	size of smallest cells	timesteps per rotor revolution
coarse	55.5/R	350
medium	83.3/R	525
fine	125.0/R	800

Blade Airloads

During the HART II test programme, the sectional airload, C_N, at a radial station of 87% was estimated by integrating the measured pressures from sensors surrounding this section of the blade. 2048 readings per rotor revolution were taken at every pressure sensor, allowing the high-frequency content of the airload to be resolved without significant aliasing.

Part (a) of Fig. 2 compares the measured blade airload at this radial station, expressed in terms of non-dimensionalised normal force coefficient ($C_N M^2$), to the airload predicted by the VTM using each of the three different resolutions of the flow field defined in Table 2. Parts (b) and (c) of the same figure show the data after filtering at 10/rev to separate the signal into the low-frequency component that is associated primarily with control input and structural deformation of the blades, and the high-frequency component that is almost exclusively associated with the BVI-induced component of the loading. The BVI-induced loading fields on the retreating and advancing sides of the rotor are reproduced with expanded azimuthal scale in Fig. 3 to aid in their interpretation. On the advancing side of the rotor disc, all BVI events that are present in the experimental data are captured by the numerics, but there are errors in the phasing and amplitude of the BVI-induced loading peaks. Increasing the resolution of the calculation reduces the errors in phase and in amplitude, increasing the accuracy of the prediction on this side of the disc. The BVI events present in the experimental data for the retreating side of the rotor are captured with the correct position, impulse width and amplitude by the coarse calculation, whereas the calculations at finer resolution significantly over-predict the amplitude of the loading that is induced by the BVI events.

It is thought that this over-prediction may be due to two different features of the VTM. Firstly, the Weissinger-L model for the blade aerodynamics is known not to predict well any loading perturbations that are associated with flow features that have similar spatial extent to the size of the panels — this becomes a significant problem only when the description

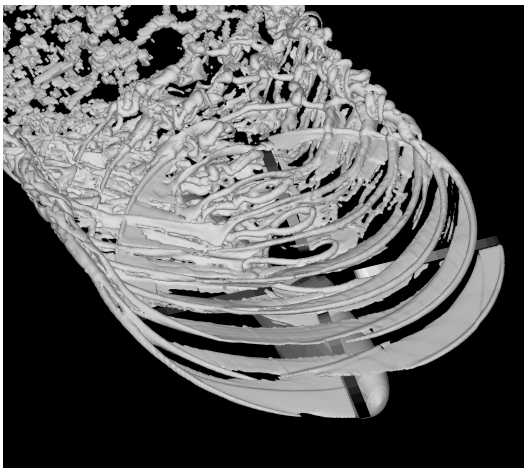

(a) *VTM computation using a fine resolution*

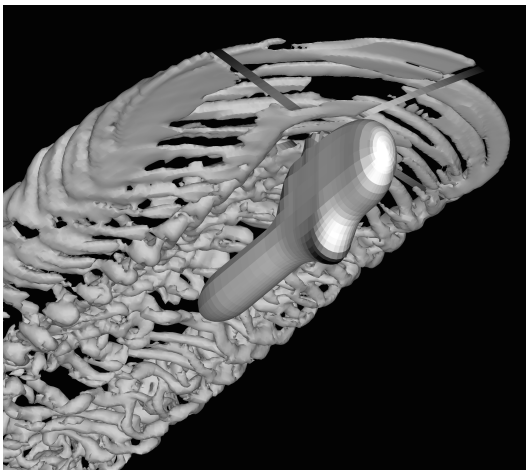

(b) *VTM computation using a medium resolution*

Figure 4: *Visualisation of the VTM-predicted wake geometry for the Baseline HART II case.*

of the wake is refined significantly but could feasibly be rectified by increasing both the chordwise and spanwise density of panels on the blade. Alternatively, the lifting-line model could be replaced using a more physically representative model for the aerodynamics near the surface of the blade, for instance using the hybrid primitive-variable CFD-VTM method proposed by Whitehouse *et al.* (Ref. 14). Secondly, no viscous model was implemented in the present calculations - this approximation has been justified in previous work using the VTM on the basis that the Reynolds number of the rotor flow has generally been too high for any physical diffusion process to be represented properly given the overwhelming effect of the numerical diffusion that is inevitably present within the calculation. At the highest computational resolution for which data is presented here though it is possible that the balance between physical and numerical diffusion may be different to that at lower computational reso-

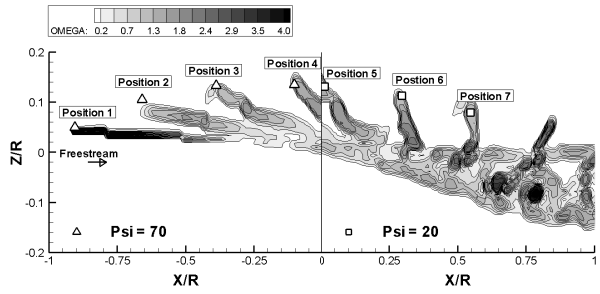

(a) *Advancing side of the rotor disc: Y/R = 0.403*

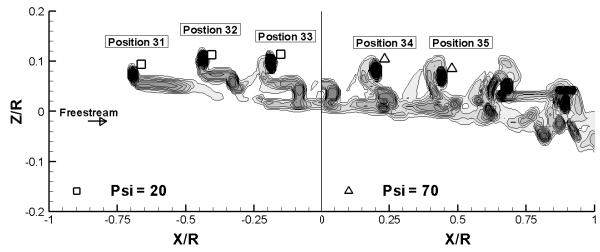

(b) *Retreating side of the rotor disc: Y/R = -0.4*

Figure 5: *Computed structure of wake vorticity (contours) and measured vortex core positions (symbols) compared on longitudinal slices through the wake (Baseline HART II case, $Y/R = \pm 0.4$, fine computational resolution).*

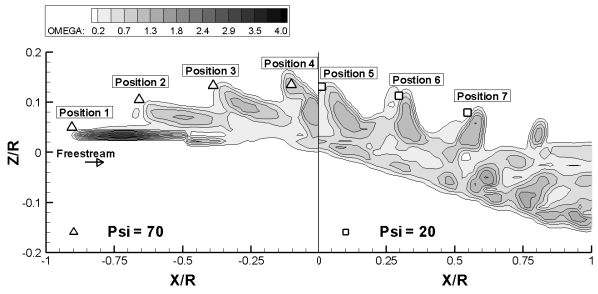

(a) *Advancing side of the rotor disc: Y/R = 0.403*

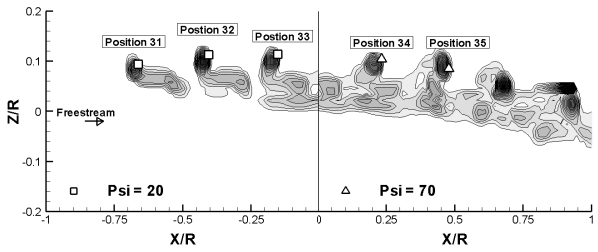

(b) *Retreating side of the rotor disc: Y/R = -0.4*

Figure 7: *Computed structure of wake vorticity (contours) and measured vortex core positions (symbols) compared on longitudinal slices through the wake (Baseline HART II case, $Y/R = \pm 0.4$, medium computational resolution).*

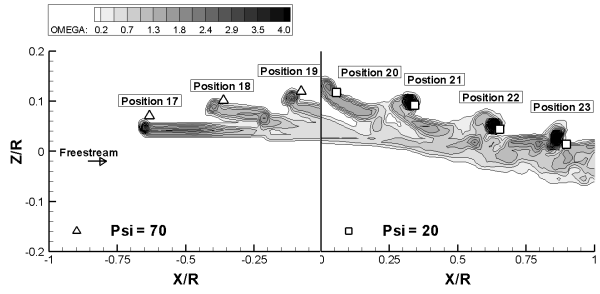

(a) *Advancing side of the rotor disc: Y/R = 0.7*

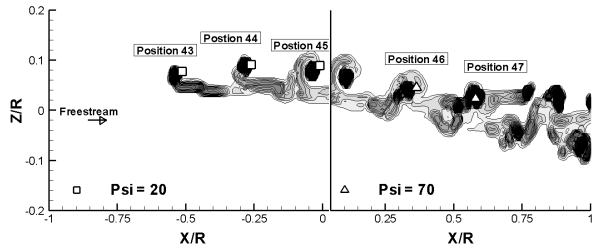

(b) *Retreating side of the rotor disc: Y/R = -0.7*

Figure 6: *Computed structure of wake vorticity (contours) and measured vortex core positions (symbols) compared on longitudinal slices through the wake (Baseline HART II case, $Y/R = \pm 0.7$, fine computational resolution).*

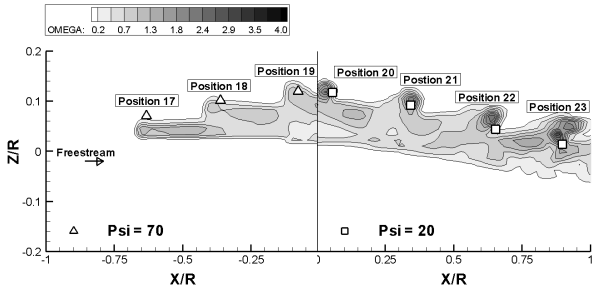

(a) *Advancing side of the rotor disc: Y/R = 0.7*

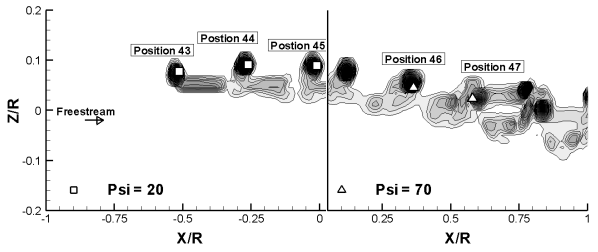

(b) *Retreating side of the rotor disc: Y/R = -0.7*

Figure 8: *Computed structure of wake vorticity (contours) and measured vortex core positions (symbols) compared on longitudinal slices through the wake (Baseline HART II case, $Y/R = \pm 0.7$, medium computational resolution).*

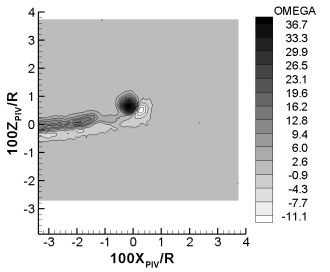

(a) *Measured vorticity field*

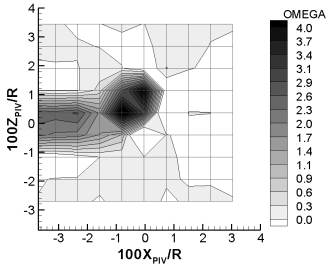

(b) *Measured vorticity field (resolution reduced to be comparable to fine computation)*

Figure 9: *Experimental vorticity distribution at the resolution of the PIV experimental data compared to experimental data where the resolution has been reduced to be comparable to that of the fine computation. (Position 17a, i.e. vortex age* 5.3°*).*

lution and thus that the physical diffusion within the system might need to be accounted for more carefully. This character of the model is likely to be exacerbated by the behaviour of the flux limiters that have been used within the WAF method to retain the integrity of the vortical structures in the wake. The possibility cannot be excluded that, in the present calculations, the limiters act to maintain a very tight, but possibly an unphysical, core structure to the individual vortices in the wake. In the next sections of the paper this hypothesis will be tested, and the ability of the present numerical approach to represent and preserve the fine-scale structure of the wake, albeit in the absence of a model for the viscous diffusion within the flow, will be discussed. A detailed study of the interrelationship between the viscous terms and the action of the flux limiters will thus be deferred to a future paper.

Wake Structure

To investigate the link between the computational resolution of the fine detail of the wake structure and the resultant accuracy of the predicted blade airloads, the VTM-predicted position and strength of the wake of the HART II rotor was compared against the HART II experimental data at a number of locations at which detailed PIV observations of the flow field were available. The geometry of the predicted wake of the HART II system, as visualised by plotting a surface in the flow on which the vorticity has constant magnitude, is depicted in Fig. 4. This figure illustrates well the characteristic behaviour of the VTM in retaining the spatial compactness of the vortical structures that are present in the flow even after numerous rotor revolutions have elapsed. The relatively strong root-vortex structure, as well as the broad vortex sheet that is generated behind the blades as they traverse the advancing side of the rotor can be seen clearly. The image also reveals some detail of how this outboard sheet eventually rolls up to form a concentrated tip vortex only some distance behind the blades, particularly on the advancing side of the rotor.

Vortex trajectories

During the HART II test, measurements of the rotor wake structure and trajectory were gathered using 3C-PIV at a series of discrete locations along five longitudinal slices through the flow between Y/R = 0.4 and Y/R = 0.97 as indicated in Fig. 1. The PIV measurement planes were oriented at 149.35° with respect to the longitudinal axis of the wind tunnel on the advancing side of the rotor and at 30.06° on the retreating side. (In the right-handed hub coordinate system Z is positive upwards and X is positive aft. The rotor hub is located at the origin of the coordinate system.) Figures 5 to 8 compare contour plots of vorticity magnitude, as predicted by the VTM, against experimental measurements of the positions of the vortex cores on a sample of these longitudinal slices.

To avoid the rotor blades from obscuring the images, the PIV measurements at locations in the first and third quadrants were collected with the rotor at 20° azimuth, and, at locations in the second and fourth quadrants, with the rotor at 70° azimuth. This difference accounts for the misalignment of the contours between the forward and aft sections of the rotor disc that is visible in the figures. Time lags in the data acquisition system gave an error of 3.5° in the measured azimuthal position of the rotor, but this has been accounted for in the presentation of the data. The measured positions of the vortex centres are plotted in Figs. 5 to 8 as symbols, and are labelled with a number corresponding to the location of the PIV measurement plane as defined in Fig. 1. The positions of the vortex centres were identified from the simple average of approximately 100 PIV images of size 0.45m

by 0.38m (0.225R by 0.19R) as described in Ref. 15.

These figures illustrate well the ability of the model to capture the geometry of the rotor wake and in particular the trajectories of the tip vortices as they are convected backwards and through the rotor disc. The locations of the maxima in the computed vorticity distribution in the wake show, in general, very good correlation with the experimentally measured vortex positions on both the slices close to the hub and those further outboard. For the forward half of the rotor disc the prediction is consistently better on the retreating side than on the advancing side of the rotor, which is consistent with the blade airload predictions, although such a trend is less obvious toward the rear of the rotor disc. Indeed, the positions of the vorticity maxima, as predicted by the VTM, are all well within one chord length (c/R = 0.0605) of the experimentally measured positions of the vortex cores. A comparison of the results for medium and fine resolutions of the computational domain shows that an increase in the spatial resolution of the flow-field results in a markedly improved definition of the various vortical structures within the wake, but does not alter significantly the predicted positions of the vortex cores within the flow. The exception is on the advancing side of the rotor, particularly at Y/R = 0.4, where a refinement of the computational mesh reduces the error in the prediction of the positions of the vortex cores from about one third of the blade chord to within the resolution of the plotted data. In Kelly *et al.*'s earlier analysis of the HART II system (Ref. 5), it was surmised that problems in resolving the BVI-induced loading on the advancing side of the rotor could be due to misrepresentation of the root vortex system that is generated by the rotor (perhaps as a result of the omission of any representation of the blade attachments or rotor hub in the simulations) and hence its effect in distorting the more outboard sections of the wake. This interpretation seems unlikely in the light of the data presented here. On the other hand, cross referencing the predictions of blade loading with the data presented in this section does suggest a consistency between the small improvement in vortex position that results from an increase in the resolution of the wake and a slight improvement in the phasing of the BVI-induced loading on the advancing side of the rotor disc.

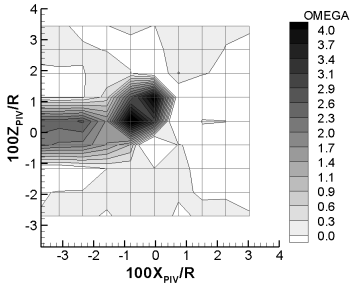

(a) *Measured vorticity field (resolution reduced to be comparable to fine computation)*

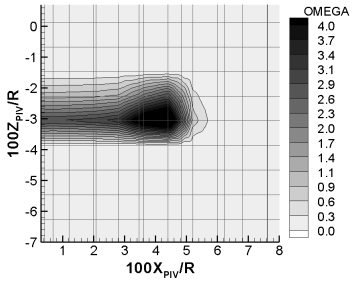

(b) *VTM computation using a fine resolution*

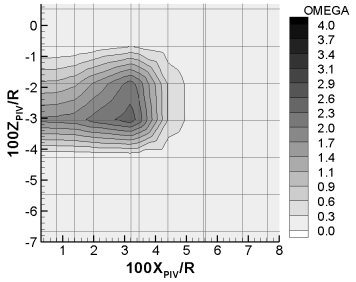

(c) *VTM computation using a medium resolution*

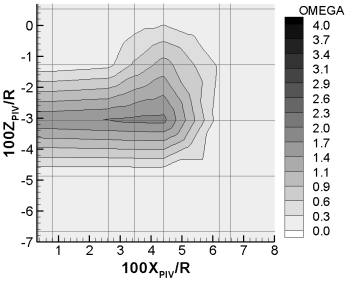

(d) *VTM computation using a coarse resolution*

Figure 10: *Vorticity distribution on the PIV plane located at position 17a (vortex age* 5.3°).

Vortex rollup

The same comparison suggests though that resolution of the positions of the vortices in the wake, even to the accuracy of a fraction of a chord-length as demonstrated in the previous section, might not be sufficient for accurate prediction of the BVI-induced loading on the rotor. It is well known that finer-scale convective

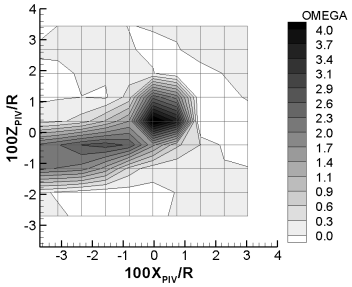

(a) *Measured vorticity field (resolution reduced to be comparable to fine computation)*

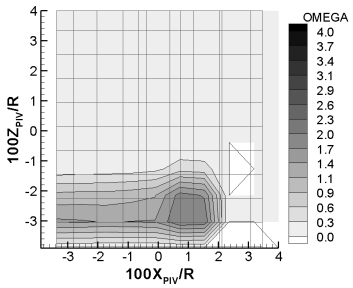

(b) *VTM computation using a fine resolution*

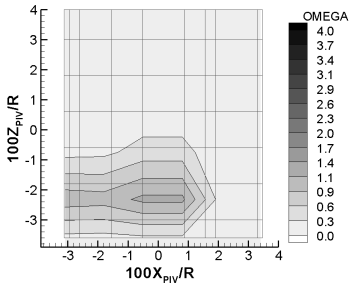

(c) *VTM computation using a medium resolution*

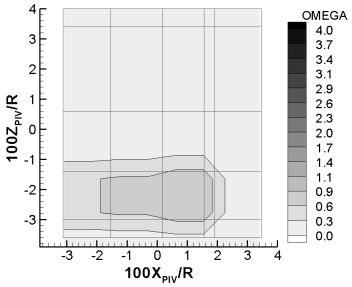

(d) *VTM computation using a coarse resolution*

Figure 11: *Vorticity field on the advancing side of the rotor, at a wake age of* 25.3° *(Baseline HART II case, position 17).*

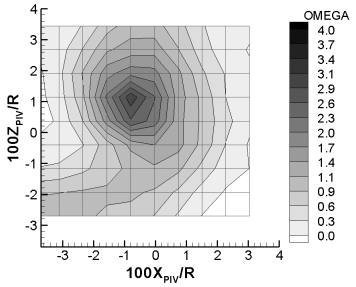

(a) *Measured vorticity field (resolution reduced to be comparable to fine computation)*

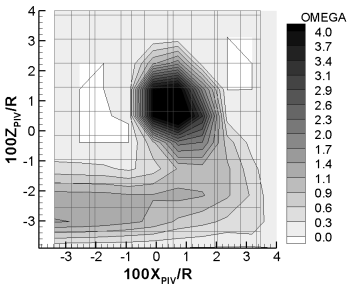

(b) *VTM computation using a fine resolution*

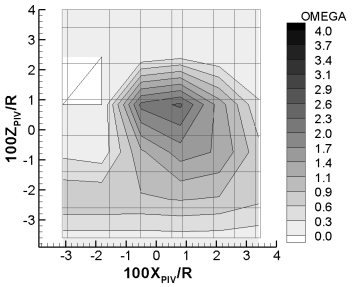

(c) *VTM computation using a medium resolution*

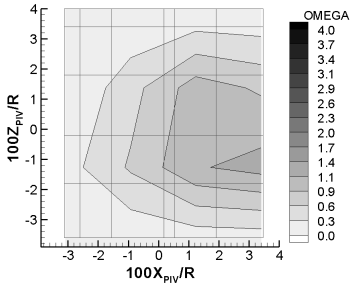

(d) *VTM computation using a coarse resolution*

Figure 12: *Vorticity field on the advancing side of the rotor, at a wake age of* 245.3° *(Baseline HART II case, position 20).*

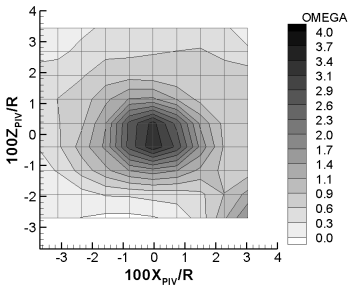

(a) *Measured vorticity field (resolution reduced to be comparable to fine computation)*

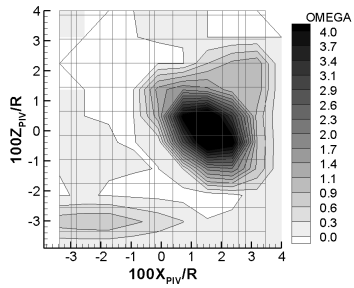

(b) *VTM computation using a fine resolution*

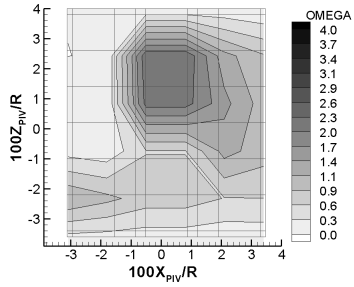

(c) *VTM computation using a medium resolution*

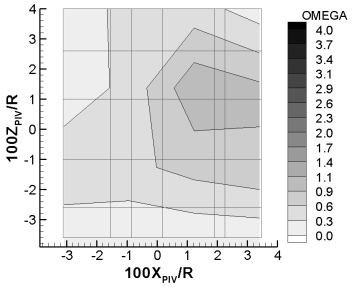

(d) *VTM computation using a coarse resolution*

Figure 13: *Vorticity field on the advancing side of the rotor, at a wake age of* 425.3° *(Baseline HART II case, position 22).*

and diffusive processes within the wake influence the distribution of the vorticity on the length-scale of the vortex core (see, for instance, Ref. 16) and are likely, if incorrectly represented, to result in significant errors in the prediction of BVI. For concentrated vortical structures, accurate resolution of the fine-scale structure is especially important where the miss-distance between the vortex and the blade is very small, but, on the other hand, detailed structural effects wash out quite quickly with increasing miss-distance because of the properties of the Biot-Savart relationship between the velocity and the vorticity. Indeed, given the descending flight condition that was modelled during the tests (and as can be inferred from the vortex trajectories shown in Figs. 5 to 8) very few of the BVI events on the HART II rotor are due to close interactions between the vortices and the blades. Where extended vortex structures are involved, however, it is possible that predictions of BVI-induced loading may be adversely affected by poor resolution of the fine-scale distribution of the vorticity in the wake even where miss-distances are significantly larger. Indeed, a possible cause of the discrepancy in resolution of the BVI-induced airloads on the advancing side of the rotor put forward in Kelly *et al.*'s earlier study of the HART II system (Ref. 5), given the rather unusual character of the tip vortices in the HART II tests, was a possible under-resolution of the process whereby the tip vortex of the blades on the advancing side of the rotor is formed, and hence a slight mis-distribution of the vorticity within the trailing vortex structure behind the blades.

The formation of the blade-tip vortices of the HART II rotor is known to be an extremely complex process. The flight condition of the baseline HART II case, combined with the twist distribution on the blades, results in a very flat loading profile along the span of the blade as it traverses the advancing side of the rotor. The vorticity that is deposited into the flow immediately behind the trailing edge of the blade thus forms a broad sheet, with relatively weak but uniform strength across its width, rather than a concentrated vortex. This sheet of vorticity then takes some time to roll up, forming a compact tip vortex only after about one quarter of a revolution of the rotor has elapsed. During the HART II experiment, a series of flow measurements were thus devoted to tracking the evolution of the vortex sheet near the tips of the blades on the advancing side of the rotor. A sequence of PIV measurements at time intervals corresponding to 5° of rotor azimuth were captured on a single observation plane (plane 17 in Fig. 1) behind the advancing blade in order to track the structure of the vortex sheet from its creation to its eventual rollup to form a compact vortical structure. A number of similar measurements

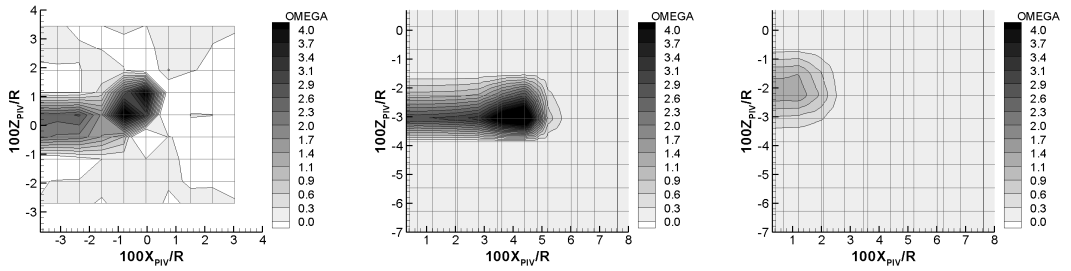

(a) *Measured vorticity field (resolution reduced to be comparable to fine computation)*

(b) *VTM Computation - Blade 1*

(c) *VTM Computation - Blade 2*

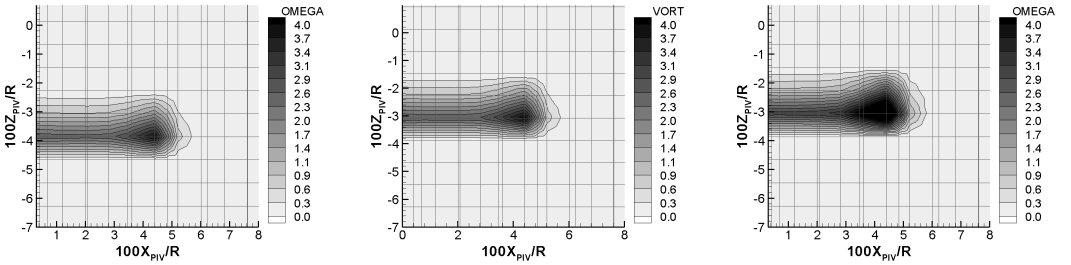

(d) *VTM Computation - Blade 3*

(e) *VTM Computation - Blade 4*

(f) *VTM Computation - Blade 1 + 1 rotor revolution*

Figure 14: *Vorticity distribution on an observation plane located at a vortex age of* 5.3° *behind each blade of the HART II rotor, showing the blade-to-blade variability of the wake structure.*

were taken on observation planes further downstream to allow the structure of the tip vortex to be investigated well after the initial rollup process had run to completion (see Fig. 1).

This data can be exploited very effectively to address the question of how well the very fine-scale processes that occur within the wake of the rotor are represented within the VTM. The evolution of the VTM-predicted vorticity distribution on this observation plane was thus compared against this experimental data in order to assess the ability of the VTM to capture both quantitatively and qualitatively the rollup of the vortex sheet behind the blades on the advancing side of the HART II rotor. The vorticity component normal to the measurement plane was extracted from the numerical data by suitable interrogation of the three-dimensional vorticity field surrounding the rotor, and was estimated from the experimental PIV data by numerical differentiation of the measured velocity field.

Figure 9 shows a sample comparison between the experimental vorticity distribution at the full resolution of the PIV measurements, and when re-sampled at the resolution of the finest grid used in the simulations. In the plots that follow, it will be more instructive to compare the VTM-predicted vorticity distributions with experimental data that has been re-sampled in this way. Figure 10 compares the predicted and measured structures of the vorticity distribution at a very early age — just 5.3° after the blade has passed through the observation plane. Note that some shifting of the numerical observation plane relative to the experimental one has been necessary to capture fully the vorticity concentration associated with the core of the tip vortex. The anomalies in the predicted tip vortex trajectory that make this shift necessary will be discussed in more detail below. The experimental measurements show the beginnings of a concentrated tip vortex just outboard of a well-defined inboard wake sheet. Qualitatively, the structure of the measured vorticity distribution is very well captured by the VTM, particularly as the resolution of the calculation is increased. The grid-lines on the plots of predicted vorticity distribution coincide with

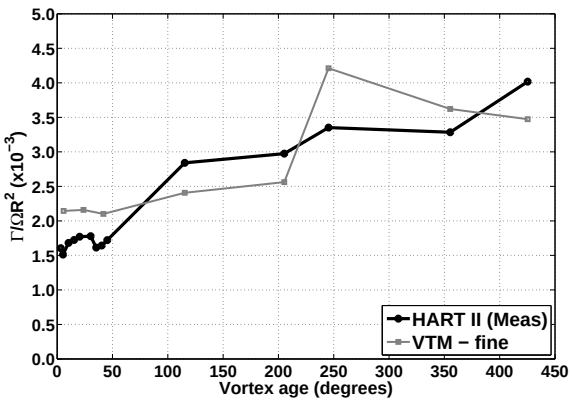

Figure 15: *Variation of tip vortex circulation with wake age (Advancing side of the rotor disc, baseline HART II case).*

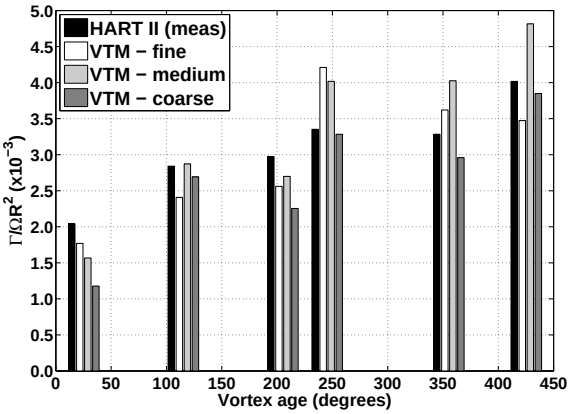

Figure 16: *Variation of the tip vortex circulation with wake age for various computational resolutions (Advancing side of the rotor disc, baseline HART II case).*

the boundaries of the computational cells*, and it is seen that the discretisation does impose some limits on the subtlety of the features that can be resolved — for instance the slight curvature of the inboard sheet is not particularly well captured by the numerics. Figure 11 presents a similar comparison of the vorticity distribution behind the blade at a somewhat later age (25.3°) during the rollup process. Figures 12 and 13 present the wake structure at a significantly later age (245.3° and 425.3°, in other words, planes 20 and 22 in Fig. 1) once the vortex sheet behind the rotor blade has almost entirely concentrated into a coherent tip vortex (no shifting of the observation plane is necessary in these cases to capture fully the vortex core). These figures show again the very good qualitative agreement between predictions and the measured shape and size of the tip vortex and inboard sheet as this structure evolves to form a coherent vortex, but some small geometric anomalies, particularly in the shape of the evolving vortex sheet, are present that appear to be consistent with the imposition of the underlying rectangular topology of the grid on the evolution of essentially arc-like vortical features within the flow.

The calculations suggest quite significant blade-to-blade variability to exist in the structure of the tip vortex. Figure 14 shows the numerical predictions of the vortical structure 5.3° behind each of the four blades of the HART II rotor. This variability is entirely due to the slightly different structural dynamics of each of the blades, but confirmation of the numerical predictions, in particular of the curiously weak structure that is created behind 'blade 2,' awaits release of more of the HART II data into the public domain. In contrast, a comparison of parts (b) and (e) of this figure reveals very little variability from revolution to revolution in the predicted structure of the wake, illustrating the convergence of the calculations onto a robust and repeatable trim state.

Several somewhat more objective measures of the development of the tip vortex can be extracted from the data to allow more rigorous assessment of the capabilities of the numerical method. The change in circulation of the tip vortex with age can be estimated (subject to certain caveats regarding the strength of the associated vortex sheet) by integrating the vorticity distribution over the area of each observation plane. Figure 15 shows that the numerical approach is able to track the measured circulation of the tip vortex extremely well, even to relatively large wake ages. Figure 16 shows furthermore that the predicted circulation of the tip vortex is relatively insensitive to grid resolution. The ability to capture the overall strength of the vortex and to convect the vorticity without significant dissipation in a manner that is relatively independent of the discretisation of the computational domain is one of the prime strengths of the vorticity-conserving approach that is implemented within the VTM.

The change in core size of the tip vortex with age can be estimated from the vorticity distributions after assuming a specific profile for the vorticity distribution within the vortex. An Oseen vortex profile (in other words a normal distribution of vorticity within the tip vortex) generally provides a good fit to the vortical structures that are predicted by the VTM, particularly where they are somewhat under-resolved by the computational grid. Assuming the Oseen profile to be appropriate, the core radius, r_c of the vortices can be estimated, in terms of the circulation Γ and the peak value of vorticity ω_{max}, in the vortex

*The unnevenness of the lines is a consequence of the PIV observation planes cutting obliquely across the underlying VTM cell structure.

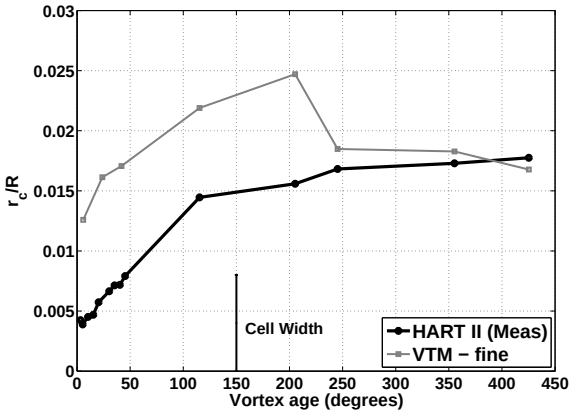

Figure 17: *Variation of the vortex core radius with wake age (Advancing side of the rotor disc, baseline HART II case).*

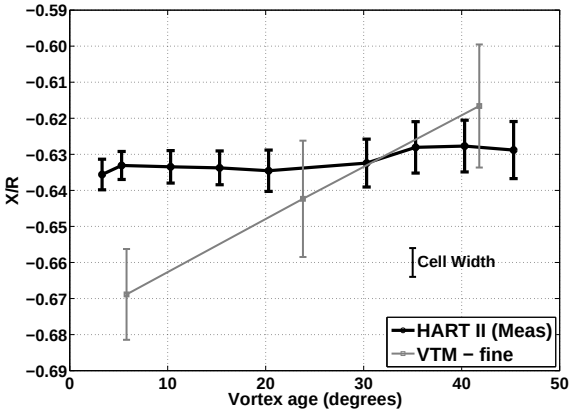

(a) *Longitudinal position of the vortex with respect to the rotor centre*

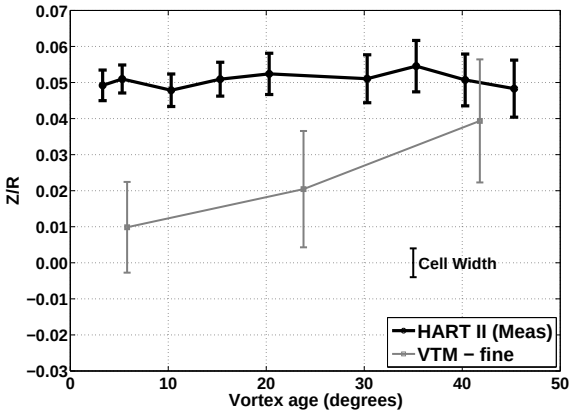

(b) *Vertical position of the vortex with respect to the rotor centre*

Figure 18: *Position of the vortex core as a function of wake age on the advancing side of the rotor disc. Bars attached to data represent the size of the vortex core. (Baseline HART II case, position 17).*

as $r_c/R = \sqrt{0.400\,|\Gamma/\omega_{max}R^2|}$. The variation in core radius with age that is obtained by analysis of the experimental data is compared in Fig. 17 to similar estimates obtained from simulations using the VTM. The rate of growth of the vortex during the initial stages of the rollup process is predicted exceptionally well by the VTM, implying that the entrainment of the inboard sheet into the developing tip vortex is accurately represented by the method. Even at the finest computational resolution attempted here, however, the radius of the vortex at very early age is about double the measured value, and hence the calculation must be considered to be under-resolved. The rather sudden contraction of the radius of the vortex at a wake age of about 200° is a fairly well-understood characteristic of the WAF method, and is caused by the interaction of the flux limiters with the underlying computational grid to form a stable (soliton-like) solution to the vortex structure that spans a particular integer number of cells. The number of cells is dependent on the exact type of limiter that is used in the calculation. Not much should thus be read into the very close agreement between the measured and predicted core sizes post this contraction since it most likely is a fortuitous coincidence between the measured profile and the cell size used in the computation.

Finally, the position of the centre of the developing tip vortex as a function of wake age can be estimated by determining the location of the point of maximum vorticity on each of the PIV observation planes. This is plotted in Fig. 18 where it is seen that the computed trajectory of the vortex follows fairly closely the trajectory that is measured experimentally. An initial offset in the vortex position of about half a blade chord appears to be a result of the finite discretisation of the surface of the blade into panels, and a small resultant positional inaccuracy in the interpolation of the vorticity into the computational domain. No doubt this inaccuracy is a contributor to the small discrepancies in the vortex positions that manifest further downstream in the wake, as shown in Figs. 5 to 8. The bars attached to the data represent the estimated size of the vortex core and, given the relatively coarse discretisation of the vortex location that is imposed by the relatively coarse resolution of the grid compared to the diameter of the vortex, the close agreement in the predicted and measured trajectories of the wake at the very early wake ages shown in the figure is encouraging nevertheless.

Conclusion

The Vorticity Transport Model (VTM) has been used to predict the wake structure for the rotor that was studied during the HART II experimental pro-

gramme. The rotor that was used in this programme was a scaled representation of the Bö 105 rotor, and was flown in a descending flight condition in which the loading on the rotor contains significant high-frequency content due to the presence of blade vortex interactions. During the experimental programme, detailed PIV images of the structure within the rotor wake were captured at various locations within the flow. This data has been used in the present paper to analyse the ability of the VTM to capture the detailed geometry of the rotor wake in order to investigate the origin of various deficiencies in the prediction of the high frequency, BVI-induced loading on the rotors that were exposed in an earlier study by Kelly *et al.* (Ref. 5). These deficiencies were largely confined to the advancing side of the rotor, where it is known that the tip vortices of the blades are formed through a particularly complex rollup process.

Calculations at three different spatial and temporal resolutions were performed, using a version of the VTM in which the dynamics of the blades could be prescribed to follow the experimentally-measured structural deformations of the system. This approach allowed any effects on the quality of the simulation that are due to mis-representation the blade dynamics to be separated from those that are induced by the aerodynamics of the system.

As expected, the quality of the prediction of the low-frequency component of the blade loading is negligibly influenced by the computational resolution of the structure of the wake once a certain minimum resolution is exceeded. The high-frequency, BVI-induced component of the loading is very sensitive to the cell size used in the computations, however. Although their phase and impulse width is marginally influenced, the predicted amplitude of the BVI-induced spikes in the loading on the blades increases significantly as the cell size that is used to resolve the wake is reduced.

Yet the predictions of the geometry of the wake are shown to match very closely the experimental data. The predicted positions of the vortex cores on two longitudinal slices through the flow, one situated close to the rotor hub and further outboard along the blade span agree with the measured data to within a fraction of the blade chord. Qualitative analysis of the rollup process in the wake of the blades on the advancing side of the rotor shows the formation of a coherent tip vortex from an extended sheet of vorticity to be captured rather well. Detailed analysis of the circulation that is induced by the tip vortices shows the vorticity conserving properties of the VTM to result in the integrity of the vortical structures in the wake being preserved to well downstream of the rotor. This property of the method has been demonstrated to be markedly independent of the resolution of the computation.

The size of the computational cells poses a fundamental lower bound on the size of the vortex that can be resolved. Thus, the calculations at even the highest resolution described here overpredict the size of the tip vortex during its initial formation by a factor of two. Calculations at higher resolution than those attempted here will soon be feasible, and it is quite likely, given the action of the flux limiters within the convective algorithm of the VTM, that future increases in resolution will result in further localisation of the vortices. In the absence of any process, such as viscous diffusion, that might counter their effect, the grid dependent, soliton-like properties of the wake structure that are induced by the flux limiters (some hint of which was seen in the predictions of vortex core radius) may result in vortex localisation to the point where the structures that are produced are unphysically small. This will need to be addressed in the very near future using a model for the dissipative mechanisms within the wake that does not interfere with the beneficial characteristics of the approach that allow it to preserve the integrity of the structure in the wake for the very long times needed to resolve blade-vortex and similar interactions within the helicopter system.

In conclusion, then, the most significant clue to the origin of the deficiencies in predicting the BVI-induced loading on the HART II rotor that were exposed in the previous study by Kelly *et al.* lies in the fact that the various cell sizes used in the present study allow the amplitude of the BVI-induced loading features on the rotor to be bracketed. In the calculation at coarsest resolution, the amplitude of the features is underpredicted on the advancing side of the rotor but close agreement with the experimentally measured peak loading is obtained on the retreating side of the rotor. In contrast, the calculation at finest resolution gives a close match with the measured amplitudes on the advancing side of the rotor but overpredicts the amplitude of the BVI-induced features in the loading on the retreating side of the rotor. This shows that the deficiencies within the prediction were not simply the consequence of the simulations inherently under-resolving the flow, for instance — in fact the vortex core sizes produced during the simulations with finest resolution of the flow were shown to be closely comparable with those of the real system (even if not for entirely the right reasons). The discrepancies between simulation and experiment are more likely due to an inherent misrepresentation of the aerodynamic response of the blade when subjected to the very localised perturbations in its aerodynamic environment that the calculations at the finest resolution of the structure of the wake are capable of producing. The

use of a lifting-line type approach where the blade chord is approximately eight times the cell size, as was the case in the most finely-resolved calculations presented here, stretches somewhat the assumptions that are inherent within the model. It will not be good scientific practice, no matter how attractive, to adopt the simple expedient of tailoring the cell size to the rotor dimensions, however — this does not result in a truly convergent numerical technique — and hence future work will concentrate on improving the localised modelling of the blade aerodynamics within the VTM framework. A particularly promising candidate in this respect is the hybrid primitive variable VTM approach advocated in Ref. 14.

References

1. van der Wall, B., Junker, B., Burley, C., Brooks, T., Yu, Y., Tung, C., Raffel, M., Richard, H., Wagner, W., Mercker, E., Pengel, K., Holthusen, H., Beaumier, P., and Delrieux, Y., "The HART II test in the LLF of the DNW - a Major Step towards Rotor Wake Understanding," *Proceedings of the 28th European Rotorcraft Forum*, Bristol, England, 2002.

2. van der Wall, B., Burley, C., Yu, Y., Richard, H., Pengel, K., and Beaumier, P., "The HART II test - Measurement of helicopter rotor wakes," *Aerospace Science and Technology*, Vol. 8, No. 4, 2004, pp. 273 – 284.

3. Lim, J., Tung, C., Yu, Y., Burley, C., Brooks, T., Boyd, D., van der Wall, B., Schneider, O., Richard, H., Raffel, M., Beaumier, P., Delrieux, Y., Pengel, K., and Mercker, E., "HARTII: Prediction of Blade-Vortex Interaction Loading," *Proceedings of the 29th European Rotorcraft Forum*, Friedrichshafen, Germany, 2003.

4. Yu, Y., Tung, C., van der Wall, B., Pausder, H.-J., Burley, C., Brooks, T., Beaumier, P., Delrieux, Y., Mercker, E., and Pengel, K., "The HART-II Test: Rotor Wakes and Aeroacoustics with Higher-Harmonic Pitch Control (HHC) Inputs - The Joint German/French/Dutch/US Project," *Proceedings of the American Helicopter Society 58th Annual Forum*, Montreal, Canada, 2002.

5. Kelly, M., Duraisamy, K., and Brown, R., "Predicting Blade Vortex Interaction, Airloads and Acoustics using the Vorticity Transport Model," *Proceedings of the American Helicopter Society 9th Aeromechanics Specialist Meeting*, San Francisco, USA, 2008.

6. Brown, R. and Line, A., "Efficient High-Resolution Wake Modelling using the Vorticity Transport Model," *AIAA Journal*, Vol. 43, No. 7, 2005.

7. Brown, R., "Rotor Wake Modeling for Flight Dynamic Simulation of Helicopters," *AIAA Journal*, Vol. 38, No. 1, 2000.

8. Toro, E., "A Weighted Average Flux Method for Hyperbolic Conservation Laws," *Proceedings of the Royal Society of London, Series A: Mathematical and Physical Sciences*, Vol. 423, 1989, pp. 401–418.

9. Kenyon, A. and Brown, R., "Wake Dynamics and Rotor - Fuselage Aerodynamic Interactions," *Proceedings of the American Helicopter Society 63rd Annual Forum*, Virginia Beach, USA, 2007.

10. Schneider, O., "Analysis of SPR measurements from HART II," *Aerospace Science and Technology*, Vol. 9, No. 5, 2005, pp. 409 – 420.

11. Schneider, O., van der Wall, B. G., and Pengel, K., "HART II Blade Motion Measured by Stereo Pattern Recognition (SPR)," *Proceedings of the American Helicopter Society 59th Annual Forum*, Phoenix, Arizona, 2003.

12. Pengel, K., Mueller, R. H. G., and van der Wall, B. G., "Stereo Pattern Recognition - the technique for reliable rotor blade deformation and twist measurement," *Proceedings of the American Helicopter Society International Meeting on Advanced Rotorcraft Technology and Life Saving Activities (Heli Japan)*, Tochigi, Utsunomiya, Japan, 2002.

13. van der Wall, B., "Mode identification and data synthesis of HART II blade deflection data," IB 111-2007/28, ftp://HART-II@ftp.dlr.de, 2007.

14. Whitehouse, G., Boschitsch, A., Quackenbush, T., Wachspress, D., and Brown, R., "Novel Eulerian Vorticity Transport Wake Module for Rotorcraft Flow Analysis," *Proceedings of the American Helicopter Society 63rd Annual Forum*, Virginia Beach, USA, 2007.

15. van der Wall, B. and Richard, H., "Analysis Methodology for 3C PIV Data," *Proceedings of the 31st European Rotorcraft Forum*, Florence, Italy, 2005.

16. Ramasamy, M., Johnson, B., and Leishman, G., "Tip Vortex Measurements Using Dual Plane Digital Particle Image Velocimetry," *Proceedings of the American Helicopter Society 64th Annual Forum*, Montreal, Canada, 2008.